Special Issue

Applied Spectroscopy

Applied Spectroscopy
2022, Vol. 76(1) 51–60

DOI: 10.1177/00037028211049242
journals.sagepub.com/home/asp
SAGE

Raman Investigation of the Processing Structure Relations in Individual Poly(ethylene terephthalate) Electrospun Fibers

Arnaud W. Laramée*, Catherine Lanthier*, and Christian Pellerin

Abstract

Electrospun fibers often exhibit enhanced properties at reduced diameters, a characteristic now widely attributed to a high molecular orientation of the polymer chains along the fiber axis. A parameter that can affect the molecular organization is the type of collector onto which fibers are electrospun. In this work, we use polarized confocal Raman spectromicroscopy to determine the incidence of the three most common types of collectors on the molecular orientation and structure in individual fibers of a broad range of diameters. Poly(ethylene terephthalate) is used as a model system for fibers of weakly crystalline polymers. A clear correlation emerges between the choice of collector, the induced molecular orientation, the fraction of trans conformers, and the degree of crystallinity within fibers. Quantitative structural information gathered by Raman contributes to a general description of the mechanism of action of the collectors based on the additional strain they exert on the forming fibers.

Keywords

Electrospinning, molecular orientation, nanofibers, Raman, molecular structure, polarized spectroscopy, processing-structure-properties relationships

Date received: 21 May 2021; accepted: 22 August 2021

Introduction

Electrospun fibers are continuous structures formed by the solidification of a thin jet propelled from a polymer solution subjected to a strong electric field.[1–4] They exhibit appealing mechanical,[5–13] electrical,[14,15] and thermal[16] properties that are often greatly enhanced at sub-micrometer diameters (d) compared to those of the bulk materials. Accordingly, they are promising materials for applications that include tissue engineering,[17–20] selective filtration,[21,22] sensing,[23] and energy harvesting.[24,25] However, our partial understanding of the processing-structure-properties relationships in electrospun fibers still limits their optimization and widespread application.[1,2,26]

Confocal Raman spectromicroscopy is a technique of choice for investigating the structure of electrospun fibers because it allows quantification of molecular and supramolecular characteristics, such as molecular orientation, conformation, and crystallinity, at the individual fiber level.[1,26–31] This structural information can then be correlated to fiber diameter, processing parameters, and to the ultimate properties. For instance, our group has shown by Raman that the molecular orientation in amorphous polystyrene fibers increases exponentially with a reduction in fiber diameter,[28] and that orientation follows the same trend as the increase in modulus.[6,7] Notably, the largest fibers presented bulk-like properties and negligible orientation while both values increased for thinner fibers below an onset diameter (d_o) value, in line with infrared spectroscopy (IR) measurements on bundles of poly(trimethyl hexamethylene terephthalamide) fibers, another amorphous polymer.[9] These orientation and mechanical

Département de chimie, Université de Montréal, Montréal, Canada
*These authors contributed equally.

Corresponding author:
Christian Pellerin, Université de Montréal CP 6128, Succ. Centre-ville, Montreal, QC H3C 3J7, Canada.
Email: c.pellerin@umontreal.ca

behaviors have been rationalized theoretically.[32–34] Recently, Raman helped evidence that the degree of crystallinity of the electrospun polymer affects the level of molecular orientation and the shape of its diameter dependence.[29] In particular, polymers with a very high degree of crystallinity, such as poly(ethylene oxide) (PEO) and poly(oxymethylene) (POM), lead to a much higher orientation throughout the diameter range and to non-zero orientation even for the largest fibers.[30] Orientation trends were also observed using other nanoscale techniques such as atomic force microscopy-IR spectroscopy[35,36] and selected area electron diffraction,[37–39] but the tedious sample preparation and analysis they require prevented studying of a sufficient number of fibers to draw definitive conclusions on diameter-dependent structural characteristics.[26] In contrast to the cases of amorphous and highly crystalline polymers, the behavior of polymers of low crystallinity, such as poly(ethylene terephthalate) (PET), remains an open question that we address herein.

An important electrospinning parameter that affects the real or apparent degree of orientation in electrospun fibers is the type of collector onto which they are deposited. Various collectors have been designed to prepare fiber mats with a macroscopic organization adapted for specific applications.[2] For instance, membranes for selective filtration generally require a random nonwoven network in which the size and density of pores must be controlled to optimize efficiency.[21,22] In this case, a simple metallic plate is usually the preferred collector. Other applications require highly aligned fibers to take advantage of their anisotropic properties, for instance in energy harvesting and electronics where alignment improves electrical transport properties,[24,25,40] or to help replicate the properties and functions of biological tissues such as promoting cell migration and growth.[17–19] The most common collectors to produce well-aligned fibers are the gap collector, which consists of conductive rods separated by a small gap and between which the fibers are quickly propelled back and forth, and the rotating collector, where fibers are mechanically drawn by the fast rotation of a metallic disk or drum. Less frequent implementations include movable setups and patterned collectors that can yield fiber mats with more complex organizations for niche applications.[20,41,42]

Up to now, most studies examining the effect of the collector on molecular orientation have been conducted at the mat level using methods such as IR spectroscopy and X-ray diffraction. At this macroscopic scale, similar observations were made for fibers spun from amorphous polymers such as polystyrene,[43] semi-crystalline polymers such as nylon-6,[44] nylon-6,6,[45] poly(acrylonitrile),[46] poly(caprolactone),[47] and poly(vinylidene fluoride) (PVDF),[48,49] as well as for highly crystalline PEO[50] and POM.[51] The apparent orientation was negligible for fibers deposited on a metallic plate, an observation mainly attributed to the absence of additional mechanical or electrostatic force exerted by the collector.[46,48–51] In contrast, aligned fibers showed a significant molecular orientation proportional, to a certain extent, to the distance between the rods for the gap collector or to the rotation velocity for the disk or drum collectors.[43–51] However, structural information obtained at the mat level depends not only on the orientation of the polymer chains but also on the alignment of fibers in the mat, leading to clear discrepancies between these studies and those conducted at the single fiber level.[1,26] Although strategies were developed to deconvolute the molecular orientation, such as maximizing the alignment or taking it into account using the Legendre addition theorem,[43,47] measurements at the mat level remain intrinsically affected by the presence of defects and by the fiber diameter polydispersity, both inherent in the electrospinning process.[1,26]

The few published studies on the effect of collection on the structure of individual fibers stand out by revealing a strong impact of the nature of the electrospun polymer that appears consistent with the above-mentioned effect of crystallinity on the diameter-dependance of orientation. Rabolt et al. showed by selected area electron diffraction that individual nanofibers of semi-crystalline PVDF and poly[(R)-3-hydroxybutyrate-co-(R)-3-hydroxyhexanoate] are significantly less oriented when collected using a metallic plate than with a rotating disk or gap collector.[48,49,52] The extent of orientation was influenced by slight variations of collector parameters that could be optimized to afford fibers with highly oriented strain-induced metastable crystal structures.[52] In sharp contrast, our group studied highly crystalline PEO fibers by Raman[53] and found that all fibers interrogated were very highly oriented regardless of the collector used (including a metallic plate). This was attributed to the fast crystallization rate of PEO that would favor the formation of highly oriented crystals before the jet reaches the collector.[30,53] These studies strongly suggest that the collection method, degree of crystallinity, and molecular orientation are interrelated and can affect the diameter-dependent properties of the resulting fibers.

In this work, we contribute to filling the gap in the understanding of the diameter- and collector-dependance of orientation for polymers of low degree of crystallinity. Fibers of PET are electrospun using the three most popular types of collectors (metallic plate, rotating disk, and gap collector) and are characterized individually by polarized Raman over a broad range of diameters. We show that the type of collector affects the shape of the diameter dependence of orientation for weakly crystalline polymers and find a correlation between the strain-induced molecular orientation, the resulting crystallinity, and the fraction of trans conformers within the fibers.

Experimental

Electrospinning

Poly(ethylene terephthalate) (PET, Scientific Polymer Products, catalogue no. 138) with an inherent viscosity of 0.58, dichloromethane (DCM, purchased from EMD), and trifluoroacetic acid (TFA, 97% Fisher Scientific) were used as received. Solutions were prepared by dissolving an appropriate mass of PET in 5 mL of a 50:50 w/w solvent mixture of DCM and TFA and agitating for 6 h to obtain concentrations ranging from 17 to 25% (m/v). After complete dissolution, the polymer solution was placed in a 5 mL glass syringe equipped with a 0.41 mm diameter flat-end needle to which a 15 kV positive voltage was applied using a CZE 1000R high-voltage power supply (Spellman High Voltage Electronics). A PHD 2000 syringe pump (Harvard Apparatus) was used to impose a constant solution flow and was generally fixed at 0.05 mL/min, with slight adjustments to ensure optimal jet formation. Fibers with d between approximately 500 and 2000 nm were spun in a fume hood at temperatures between 22 and 24 °C and at a relative humidity below 35%. They were collected using three collectors: a static aluminum foil, a gap collector consisting of two metallic rods separated by ~25 mm, and a metallic disk rotating at a linear velocity of ~450 m/min. In all cases, the working distance between the needle tip and the collector was 15 cm and a negative 2 kV potential was applied on the collector using a second power supply (Power Designs). The spinning time was adjusted to yield samples of well-isolated fibers for Raman characterization. Fibers were dried under vacuum for at least 48 h prior to analysis to minimize residual solvent and solvent-induced orientation relaxation.

Confocal Raman Microscopy

Raman spectra were acquired in the backscattering geometry using the 632.8 nm He–Ne laser of a LabRam HR800 spectrometer (Horiba Scientific) coupled with an Olympus BX41 microscope fitted with a long working distance 100 × objective (numerical aperture of 0.8). The confocal hole and the slit of the instrument were 100 and 150 μm, respectively. The polarization of the incident laser beam and the Raman scattered light was set parallel (Z) or perpendicular (X) to the fiber axis or film drawing direction by using a half-wave plate and an analyzer, respectively. A 600 grooves/mm holographic grating was used in conjunction with a scrambler to alleviate its polarization dependent diffraction efficiency.

Prior to fiber characterization, a series of cold-drawn PET films of 35 ± 5 μm thickness were analyzed to build a calibration curve allowing an efficient one-spectrum orientation quantification in individual fibers. The integration time was set to 3 s and averaged five times for each spectrum. Complete sets of parallel- and cross-polarized spectra were collected for films, in the order ZZ, ZX, XX, XZ, ZZ(2), with the second ZZ spectrum acquired to detect possible loss of focus during acquisition. Any set of spectra was rejected if the intensity of the 1616 cm^{-1} band, used for orientation quantification, differed by more than 5% between the ZZ and ZZ(2) spectra. The order parameters $\langle P_2 \rangle$ were calculated using the most probable distribution (MPD) method[54,55] and were corrected for a tilt angle of 20° between the principal axis of the Raman tensor and the polymer main chain.[56] The $\langle P_2 \rangle$ takes a value of 0 for a completely isotropic system and a maximum value of 1 for perfect orientation of the chains along the reference direction (the fiber axis or film drawing direction). The intensity ratio of the 1616 and 705 cm^{-1} bands (I_{1616}/I_{705}) in the ZZ spectrum was then plotted against $\langle P_2 \rangle$ to afford a linear calibration curve ($R^2 = 0.99$). This calibration procedure could be subject to bias in the calculated $\langle P_2 \rangle$ values if the calibration films showed a substantial degree of biaxial orientation at their surface,[57] which would not be present in the electrospun fibers. The $\langle P_2 \rangle$ values obtained at the surface and in the bulk of tested films were similar. While a bias cannot be excluded, it would be present under all conditions studied and should not affect the reported trends.

Fibers were recovered from the collectors, immobilized onto BaF_2 windows with fine tweezers and adhesive tape, and individually characterized under the ZZ polarization. The integration time was set to 10 s and averaged seven times. The $\langle P_2 \rangle$ values were obtained from the I_{1616}/I_{705} band intensity ratios and the calibration curve. The diameter of each fiber was estimated by acquiring a series of 10 to 15 ZZ spectra at regularly spaced positions perpendicular to the fiber axis. The spectral intensity was then plotted as a function of position, resulting in a bell-like distribution with an intensity maximum at the center of the fiber. The data were fitted to a Gaussian function, using Origin software, and the diameter was taken as double the computed standard deviation (σ) of the fitted function. The diameter value computed using this method is reliable for larger fibers, but it is overestimated when the fiber is thinner than the size of the laser spot. Optical effects related to the curvature of the fibers may also impact the reported diameter values because of the use of a metallurgical objective.[58] These effects should apply uniformly to all data sets and are not expected to affect the observed trends.

The fraction of trans conformers was determined on the basis of a method first developed by Rodríguez-Cabello et al.[59] and adapted in our previous study[27] to minimize the effect of orientation as:

$$F_T = P_T\left[\left(\frac{I_{998}}{I_{705}}\right)_{ZZ} + 2\left(\frac{I_{998}}{I_{705}}\right)_{XX}\right] \quad (1)$$

where P_T is a coefficient representative of the weight of the 998 cm^{-1} band relative to that of the 886 cm^{-1} band

(associated with trans and gauche conformations, respectively) whose experimental value is 0.2908. Measurements on films showed that a linear relation ($R^2 = 0.99$) exists between the F_T values determined from Eq. 1 using the ZZ and XX intensities and those determined using the ZZ intensities only. The F_T values for fibers were thus calculated from the ZZ spectra and converted to their isotropic counterpart. The crystallinity index (X_c) was calculated from the polymer density (ρ), which can be estimated in first approximation from the full width at half-maximum (FWHM) of the 1725 cm^{-1} carbonyl band ($FWHM_{1725}$) under the ZZ polarization, according to:[60]

$$\rho = \frac{-FWHM_{1725} + 305}{209} \quad (2)$$

$$X_c = (\rho - \rho_a)/(\rho_c - \rho_a) \quad (3)$$

where ρ_a and ρ_c are the densities of the amorphous and crystalline phases taken as 1.335 and 1.445 g/cm^3, respectively.[61] Although it has been shown that the $FWHM_{1725}$ measured under ZZ and XX polarizations can differ for highly oriented and/or crystalline systems,[62] thus leading to differences in X_c, our preliminary tests did not uncover a systematic bias in our data.

Results and Discussion

Molecular Orientation

Poly(ethylene terephthalate) is a ubiquitous engineering polymer whose structure and properties strongly depend on its thermomechanical history. It has an excellent electrospinnability which, combined with a good understanding of its vibrational spectra and large Raman scattering cross-section,[27,56,63–67] makes it an excellent model polymer for this study. PET can form three distinct phases: the amorphous, crystalline, and mesomorphous (also called oriented amorphous phase or mesophase) phases.[27,63] The disordered amorphous phase is dominated (~80–90%) by gauche conformers of the C–C bonds of the ethylene glycol unit, whereas the crystalline and mesomorphous phases are both associated with its trans conformation. These phases are mainly differentiated by the organization of the terephthaloyl moiety, where the carbonyls in the crystalline phase are coplanar with the phenyl ring and in trans conformation while conformational disorder is present in the mesophase.[63] As shown below, these three phases can be present in electrospun PET fibers and affect its orientation processes.

Figure 1 shows the Raman bands involved in our orientation quantification procedure, for three fibers of varying diameter and orientation collected on the gap collector. Molecular orientation at the single fiber level was quantified using the 1616 cm^{-1} band, assigned to the symmetric C=C stretching of the benzene ring.[64] This band is of particular interest because it is representative of the overall orientation as established from its constant position and bandwidth upon orientation or crystallization.[57,68] Although a series of four polarized spectra (ZZ, XX, ZX, and XZ) can be used to quantify orientation,[69] the procedure is cumbersome when a large number of fibers must be analyzed. Furthermore, we have previously shown that the $\langle P_2 \rangle$ values can be strongly inaccurate for smaller fibers with a diameter close to or below the diffraction limit due to their birefringence and surface curvature.[26,29] A calibration curve enabling faster and more reliable orientation quantification in individual fibers was thus established by relating $\langle P_2 \rangle$ values for a series of cold-drawn PET films, as calculated from series of four polarized spectra, to the 1616/705 cm^{-1} band intensity ratio under the ZZ polarization (Fig. S1, Supplemental Material), where the 705 cm^{-1} band acts as an internal reference. This calibration curve eliminates the risk of losing focus or signal drift when changing the polarization between spectral acquisitions and enables the study of submicrometer fibers.[1,26,27] More than 200 PET fibers collected on either an aluminum plate, a gap collector or a rotating disk were characterized individually.

Figure 2 shows the molecular orientation of PET fibers as a function of diameter for the three collectors. To emphasize the main trends, data are represented as median values with marks indicating the data dispersion from the 25th to the 75th percentiles (see Fig. S2 for complete data). The fibers collected with the static aluminum plate stand out as their $\langle P_2 \rangle$ values remain close to 0, with a narrow dispersion, over the entire diameter range. Even for

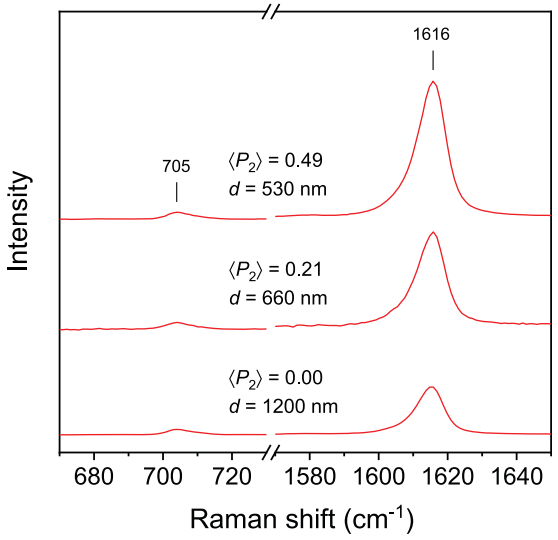

Figure 1. Spectral bands of PET used for orientation quantification, as measured on three representative individual fibers collected on the gap collector. The spectra are measured in ZZ polarization and are normalized to the 705 cm^{-1} band.

small fibers of $d < 550$ nm (those whose diameter, being under the size of the focused laser spot, is not precisely known), the median $\langle P_2 \rangle$ value is 0.02 and individual fibers do not exceed a $\langle P_2 \rangle$ of 0.04. PET fibers collected on a metal plate are therefore essentially isotropic and a possible onset diameter (d_o) for molecular orientation has not been reached. In contrast, fibers collected with the gap collector and the rotating disk show a sharp increase in orientation at reduced d. The median orientations for $d < 550$ nm are 0.18 and 0.24 for the gap collector and for the rotating disk, respectively, with individual fibers reaching values as high as 0.74 and 0.39, respectively.

The rise in orientation when $d < d_o$ is similar to previous observations for other amorphous[28,43] or semi-crystalline systems.[29,45–48,51,52] It is usually attributed to the strong elongational forces acting on the jet, where thinner fibers would originate from jets subjected to higher deformation.[1–4,22] This chain extension process competes with solvent-induced relaxation until the polymer chains become kinetically frozen, either because of crystallization or when the effective glass transition temperature ($T_{g,\ eff}$) of the polymer becomes higher than room temperature.[2,28] The higher surface-to-volume ratio of thinner fibers favors faster solvent evaporation, further contributing to their higher orientation. However, the results of Fig. 2 for the static aluminum plate indicate that the threshold for significant molecular orientation is never reached during the electrospinning process (i.e., before reaching the collector) even for fibers with the lowest d reached. Furthermore, the d_o value is higher for the rotating disk than for the gap collector, pointing to the role of the collector in orienting PET chains. The dispersion of the orientation from fiber to fiber at small d is also narrower with the rotating disk, keeping in mind that the electrospinning conditions were otherwise identical. Therefore, our data confirm that the diameter dependence of molecular orientation in electrospun fibers of low crystallinity polymers can be modulated by the collection method.

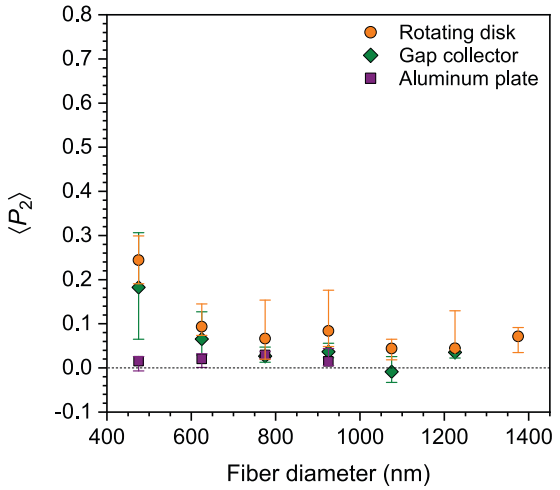

Figure 2. Diameter dependence of molecular orientation in PET fibers collected using an aluminum plate, a gap collector, and a rotating disk. The symbols represent the median of data points measured over 150 nm diameter windows and the vertical marks represent the orientation dispersion from the 25th to 75th percentiles for each window. The first data point includes fibers thinner than the laser spot so that the reported diameter may be overestimated. The full dataset is available in Fig. S2.

Molecular Structure

The ability of PET to form three distinct phases, depending on the experimental conditions, provides additional information to rationalize the effect of the collector on orientation. Figure 3a highlights Raman bands sensitive to conformation or crystallization. The 998 cm^{-1} band, associated with O−CH_2 and C−C stretching of the ethylene glycol unit in the trans conformation,[70] was used to quantify the fraction of the trans conformers (F_T) of the C–C bond of the ethylene glycol unit. It observed in the ZZ spectra of oriented fibers but is very weak in XX spectra, indicating that the chain segments in trans conformation present a high degree of orientation. The intensity of the band, and thus F_T, also increases with overall molecular orientation (see below). Conversely, the intensity of the 886 cm^{-1} band, associated with gauche conformers,[64] decreases for more oriented fibers.[61,70] This confirms that stress-induced gauche-to-trans conversion occurs during electrospinning of PET fibers, as previously observed in spin-oriented fibers and drawn films.[71] Figure 3b shows that a strong correlation exists between F_T and $\langle P_2 \rangle$ for the three collection methods. Unoriented or weakly oriented fibers have $F_T = 10$–15%, a low fraction typical of amorphous PET.[59,63] The trans fraction increases almost linearly with orientation and reaches about 40% for fibers with the highest $\langle P_2 \rangle$ values, suggesting a dominant contribution of the trans conformers to the overall orientation. Fibers collected using the aluminum foil are clustered (with few exceptions) in the region of low F_T and low $\langle P_2 \rangle$, while those collected on the gap collector or the rotating disk present a wide array of F_T (see also Fig. S3) consistent with their diameter-dependent $\langle P_2 \rangle$ values. Interestingly, fibers prepared with the rotating disk have a trans content on average 3% higher than the fibers of similar $\langle P_2 \rangle$ value collected on the gap collector.

It must be noted that while the dispersion of $\langle P_2 \rangle$ and F_T values can be quite large for fibers of a given d (see Figs. S2 and S3), the scattering of F_T versus $\langle P_2 \rangle$ in Fig. 3b is small. The pooled data for the three collectors can be fitted to a linear function with $R^2 = 0.89$, which indicates that the observed dispersion is mostly due to a real distribution of structural characteristics in individual fibers and not to large quantification uncertainty. This is well illustrated by a few individual fibers prepared on the aluminum plate that

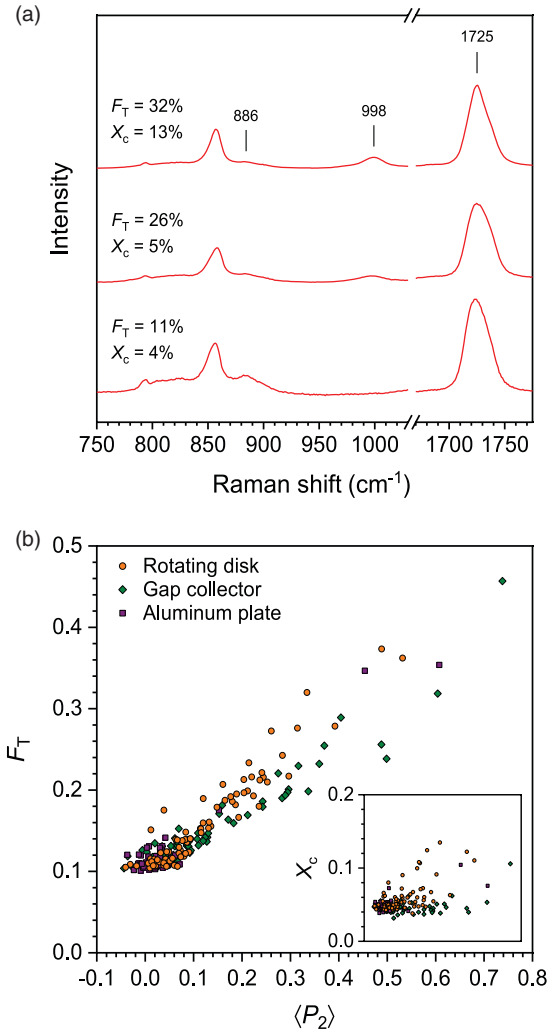

Figure 3. (a) Spectral bands of PET sensitive to crystallinity (1725 cm^{-1}), trans fraction (998 cm^{-1}), and gauche fraction (886 cm^{-1}), measured for individual fibers collected on the rotating disk (top), the gap collector (middle), and the aluminum plate (bottom). Each fiber had a diameter of ~550 nm and a $\langle P_2 \rangle$ of 0.33, 0.49, and 0.01, respectively. (b) Evolution of the fraction of trans conformers as a function of $\langle P_2 \rangle$. The inset shows the corresponding variation in the degree of crystallinity.

contain an unusually large F_T with 30% of trans conformers (highlighted in red in Fig. S3). While they are clear outliers in terms of their molecular structure, they are very well aligned with the F_T versus $\langle P_2 \rangle$ correlation in Fig. 3b.

The increase in F_T for oriented fibers can be due to crystallization or to formation of the mesophase.[63] To determine their relative contribution, we evaluated the degree of crystallinity (X_c) in each fiber using a standard approach based on the width of the carbonyl stretching band, which is narrower for the crystalline phase than for the mesomorphous or amorphous phases.[60] The inset of Fig. 3b highlights the low X_c for the vast majority of fibers, with values centered around 4–5% and never exceeding 14%. These low X_c values, compared to F_T, indicate that the stress-induced trans conformers are primarily found in the mesophase. The mesophase fraction, F_M, can be estimated as $F_M = F_T - X_c$. Figure S4 shows that the correlation between F_M and $\langle P_2 \rangle$ is closer to linearity ($R^2 = 0.93$) than for F_T, emphasizing the link between the stress-induced mesophase and the development of molecular orientation. It can be noted in the inset of Fig. 3b that fibers collected with the rotating disk tend to present a higher crystallinity than fibers prepared using the aluminum plate or the gap collector. Their average X_c value is around 7% and directly accounts for their ~3% higher F_T noted above.

Discussion

The single-fiber level Raman analyzes allow drawing a precise portrait where PET fibers can show three main internal structures:

(i) Fibers of essentially isotropic and amorphous structure, as observed for the largest fibers on either collector or for most fibers collected with the aluminum plate;
(ii) Fibers with an oriented structure, a significant mesophase fraction and a low crystallinity, as observed for most fibers of small *d* collected with the gap or rotating disk collectors;
(iii) Fibers with an oriented structure, a significant mesophase fraction and an intermediate crystallinity, as observed mainly for several fibers collected with the rotating disk.

The main observations can be rationalized by considering the effective T_g ($T_{g,\ eff}$) of the polymer jet when reaching the region where it is influenced by the collector. The electrospinning solvent acts as a plasticizer that lowers $T_{g,\ eff}$ compared to the T_g of the pure polymer (~80 °C for PET) to an extent that depends on its volume fraction. Once $T_{g,\ eff}$ exceeds room temperature (RT), due to gradual solvent evaporation, the chain mobility is strongly reduced so that the orientation or structural changes that were induced by the electrostatic stretching of the jet become frozen-in. The collector can nevertheless affect the molecular structure if it imposes sufficiently high mechanical or electrostatic forces to compensate the high viscosity of the solidified jet. The observation that fibers collected on the static aluminum plate are mainly isotropic and amorphous, irrespective of *d*, implies that the electrostatic forces were insufficient to prevent the relaxation of orientation and/or strain-induced conformational changes. Only few of these fibers (highlighted in Figs. S2 and S3) show orientation, mesophase formation and partial crystallization, presumably resulting from exceptional conditions made possible by the inherent variability in the electrospinning process.[1–4,72]

In contrast, additional electrostatic or mechanical stretching forces act on the jet when using the gap collector or the rotating disk. For the gap collector, stretching occurs when the jet undergoes a rapid back and forth motion between the rods under the action of a local electric field.[50,52,73] For fibers of low d, this enables the formation of a highly oriented mesophase which cannot relax back to the amorphous state because $T_{g,\ eff}$ is high enough when reaching the collector (keeping in mind that the low d is partially a consequence of this collector-induced stretching). This condition of $T_{g,\ eff} > RT$ also prevents rearrangement of the mesophase into the stable crystalline phase. In comparison, the rotating disk imposes tensile drawing if its linear velocity is larger than the velocity of the incoming jet. This is again sufficient to create the highly oriented mesophase for fibers of low d. However, we also observe an increase in crystallinity for some fibers, not necessarily for the thinnest ones, which can be linked to a perturbation of the jet at an earlier stage than with the gap collector. If stretching is imposed when $T_{g,\ eff}$ is still below RT, the chain mobility can be high enough to enable reorganization into the crystalline phase. These partially crystalline fibers tend to present a higher mesophase content and a substantially higher orientation than fibers of similar diameter that did not crystallize. This implies that crystallites contribute to prevent the solvent-induced orientation relaxation and conformation relaxation. We note that the few fibers prepared on the aluminum plate that show an increased degree of crystallinity also present a much higher orientation than comparable fibers that did not crystallize.

Our results on electrospun fibers are in good agreement with studies by Griffiths et al. on the step deformation of amorphous PET films, below and above T_g, using polarization modulation IR linear dichroism and ultrarapid-scanning Fourier transform IR spectroscopy.[65,66] Cold drawing below T_g, a condition comparable to the stretching of the jet with $T_{g,\ eff} > RT$, resulted in the formation of up to 60% of a highly oriented mesophase during the neck propagation without significant crystallization.[66] In contrast, drawing at temperatures just above T_g only resulted in reversible gauche-to-trans conversion and orientation due to higher chain mobility.[65] This condition is reminiscent of the electrospinning on the aluminum plate where stretching occurs mainly at $T_{g,\ eff} < RT$ and low FT and $\langle P_2 \rangle$ values are obtained. Cole et al. reported that the formation of the crystalline phase is possible when drawing films at higher temperatures with respect to T_g (or, in our case, at lower $T_{g,\ eff}$) and higher draw rates, so that the rearrangement of the terephthaloyl moiety into the crystalline structure is facilitated.[63] This occurs sporadically for electrospun PET fibers, and most frequently when using the rotating disk because it affects the jet at longer distance (where $T_{g,\ eff}$ is lower) than the other collectors.

The distinct stretching processes associated with the collectors also provide a plausible explanation for the dispersions in $\langle P_2 \rangle$ values observed in Figs. 2 and S2. The back and forth stretching process characteristic of the gap collector is prone to fluctuations in the strength and local distribution of the electric field, which depend on the amount and location of residual charges on the fibers.[50,52,73] This may cause some fibers to experience a stronger or weaker electric field and a longer or shorter path between the rods. In comparison, the continuous rotation of the disk collector ensures that the fibers are deposited around the entire circumference (32 cm) with a more uniform charge distribution.[2,43,47,50,52] A more consistent final stretching step enables a more uniform level of orientation. From a scaling-up perspective, rotating disk or drum collectors can help produce fibers with more consistent properties and repeatable performance.

Recent theoretical studies show that the ability of an electrospun fiber to develop and maintain a significant orientation depends not only on the drawing ratio imposed on the jet but also on its strain rate.[32,74] To obtain oriented fibers, the strain rate must reach a critical value where the chains undergo a transition between the coil state and the stretch state.[32,75] According to this model, d_o depends on the critical strain rate and can be estimated from an array of electrospinning parameters mainly associated with solution properties and jet initiation (which were kept constant in our study), under conditions where the system is solvated and chain mobility is significant ($T_{g,\ eff} < RT$).[32] The absence of orientation for fibers collected on the aluminum plate suggests that d_o is below the range of d covered and therefore that the critical strain rate is not reached under our electrospinning conditions. In contrast, the observable d_o and the higher fiber crystallinity associated with the rotating disk suggest that this collector can act through two mechanisms: (i) it induces the formation of the oriented mesophase by tensile drawing at the latest stage of electrospinning when $T_{g,\ eff} > RT$, and (ii) it sometimes increases the strain rate above the critical value at an earlier stage when $T_{g,\ eff} < RT$, which in turn facilitates the strain-induced crystallization by generating an appropriate molecular environment.[63,75] In this context, the gap collector, which leads to an intermediate d_o but does not increase crystallinity, would essentially act by the first of these two mechanisms.

Our results suggest that the ability of a polymer to form crystalline or organized phases during electrospinning influences the critical strain rate and d_o, and therefore the degree of orientation for fibers of a given diameter. This is most clearly seen from the unusually large orientation found for fibers exhibiting a strain-induced crystallization, even though the degree of crystallinity reached remains low. A similar behavior was witnessed in a Raman study by Papkov et al. on low crystallinity poly(acrylonitrile) fibers, where orientation remained substantial over a wide range of diameters while still showing the typical increase when $d < d_o$. In our recent studies of highly crystalline POM and PEO,[30,53] we

found that the inherent jet strain rate was sufficient to yield high orientation over a wide *d* range, regardless of the collector used or other parameters such as the electrospinning solvent. This was explained by the propensity of POM and especially of PEO to rapidly crystallize in the jet when $T_{g,\,eff} < RT$ before reaching the collector. We therefore conclude that the influence of the collectors on the fiber internal structure depends on the ability of the polymer to form stable stress-induced oriented phases in the solvent-laden jet. Amorphous or weakly crystalline polymers are therefore strongly influenced by the collector and the $T_{g,\,eff}$ at which jet deformation occurs, as observed for PET in the present study, while highly crystalline polymers are the least influenced.

Conclusion

Confocal Raman spectromicroscopy helped to unravel the effect of the collector on the molecular orientation and the internal structure in individual electrospun fibers of weakly crystalline polymers through the analysis of PET fibers collected on a metallic plate, a gap collector, and a rotating disk. The ability of PET to form three distinct (amorphous, mesomorphous, and crystalline) phases allowed a more detailed description of the mechanism of action of these broadly used collectors. Quantitative diameter-dependent measurements of orientation and phase composition at the single fiber level indicate that the gap collector and the rotating disk induce significant chain alignment through jet stretching, but that the latter exerts a more efficient and more consistent strain than the former. In contrast, a simple metallic plate collector did not induce a large enough strain rate in the electrospinning jet to induce a stable orientation in the fibers. Based on these results and our previous Raman studies of submicrometer fibers, we conclude that the influence of the collector on molecular orientation and structure depends on the intrinsic propensity of the electrospun polymer to form stable oriented phases (crystalline or mesomorphous) under strain and on the effective glass transition temperature at which the collector-induced stretching occurs. This work shows how detailed spectroscopic studies can ultimately assist the choice of collector to develop materials with targeted structure and properties.

Acknowledgments

A.W.L. and C.L. thank the Natural Science and Engineering Research Council of Canada (NSERC) and Fonds de Recherche du Québec–Nature et Technologies (FRQNT) for graduate scholarships.

Declaration of Conflicting Interests

The author(s) declared no potential conflicts of interest with respect to the research, authorship, and/or publication of this article.

Funding

The author(s) disclosed receipt of the following financial support for the research, authorship, and/or publication of this article: NSERC Grant no. RGPIN-04014-2015.

ORCID iD

Christian Pellerin https://orcid.org/0000-0001-6144-1318

Supplemental Material

All supplemental material mentioned in the text is available in the online version of the journal.

References

1. M. Richard-Lacroix, C. Pellerin. "Molecular Orientation in Electrospun Fibers: From Mats to Single Fibers". Macromolecules. 2013. 46(24): 9473–9493.
2. J. Xue, T. Wu, Y. Dai, Y. Xia. "Electrospinning and Electrospun Nanofibers: Methods, Materials, and Applications". Chem. Rev. 2019. 119(8): 5298–5415.
3. D.H. Reneker, A.L. Yarin, H. Fong, S. Koombhongse. "Bending Instability of Electrically Charged Liquid Jets of Polymer Solutions in Electrospinning". J. Appl. Phys. 2000. 87(9): 4531–4547.
4. D.H. Reneker, A.L. Yarin. "Electrospinning Jets and Polymer Nanofibers". Polymer. 2008. 49(10): 2387–2425.
5. C.-L. Pai, M.C. Boyce, G.C. Rutledge. "Mechanical Properties of Individual Electrospun PA 6(3)T Fibers and their Variation with Fiber Diameter". Polymer. 2011. 52(10): 2295–2301.
6. Y. Ji, B. Li, S. Ge, J.C. Sokolov, M.H. Rafailovich. "Structure and Nanomechanical Characterization of Electrospun PS/Clay Nanocomposite Fibers". Langmuir. 2006. 22(3): 1321–1328.
7. Y. Ji, C. Li, G. Wang, J. Koo, et al. "Confinement-Induced Super Strong PS/MWNT Composite Nanofibers". Europhys. Lett. 2008. 84(5): 56002.
8. E.P.S. Tan, C.T. Lim. "Physical Properties of a Single Polymeric Nanofiber". Appl. Phys. Lett. 2004. 84(9): 1603–1605.
9. C.-L. Pai, M.C. Boyce, G.C. Rutledge. "On the Importance of Fiber Curvature to the Elastic Moduli of Electrospun Nonwoven Fiber Meshes". Polymer. 2011. 52(26): 6126–6133.
10. D. Papkov, Y. Zou, M.N. Andalib, A. Goponenko, et al. "Simultaneously Strong and Tough Ultrafine Continuous Nanofibers". ACS Nano. 2013. 7(4): 3324–3331.
11. J.H. Park, G.C. Rutledge. "Ultrafine High Performance Polyethylene Fibers". J. Mater. Sci. 2018. 53(4): 3049–3063.
12. A. Arinstein, M. Burman, O. Gendelman, E. Zussman. "Effect of Supramolecular Structure on Polymer Nanofibre Elasticity". Nat. Nanotechnol. 2007. 2(1): 59–62.
13. R. Hu, E. Gao, Z. Xu, L. Liu, et al. "Hierarchical-Structure-Dependent High Ductility of Electrospun Polyoxymethylene Nanofibers". J. Appl. Polym. Sci. 2019. 136(8): 47086.
14. G. Ico, A. Showalter, W. Bosze, S.C. Gott, et al. "Size-Dependent Piezoelectric and Mechanical Properties of Electrospun P(VDF-TrFE) Nanofibers for Enhanced Energy Harvesting". J. Mater. Chem. A. 2016. 4(6): 2293–2304.
15. Y. Zhou, M. Freitag, J. Hone, C. Staii, et al. "Fabrication and Electrical Characterization of Polyaniline-Based Nanofibers with Diameter Below 30 nm". Appl. Phys. Lett. 2003. 83(18): 3800–3802.
16. Z. Zhong, M.C. Wingert, J. Strzalka, H.-H. Wang, et al. "Structure-Induced Enhancement of Thermal Conductivities in Electrospun Polymer Nanofibers". Nanoscale. 2014. 6(14): 8283–8291.
17. J. Xie, M.R. MacEwan, W.Z. Ray, W. Liu, et al. "Radially Aligned, Electrospun Nanofibers as Dural Substitutes for Wound Closure

and Tissue Regeneration Applications". ACS Nano. 2010. 4(9): 5027–5036.
18. J. Xie, X. Li, J. Lipner, C.N. Manning, et al. "'Aligned-to-Random' Nanofiber Scaffolds for Mimicking the Structure of the Tendon-to-Bone Insertion Site". Nanoscale. 2010. 2(6): 923–926.
19. J. Qu, D. Zhou, X. Xu, F. Zhang, et al. "Optimization of Electrospun TSF Nanofiber Alignment and Diameter to Promote Growth and Migration of Mesenchymal Stem Cells". Appl. Surf. Sci. 2012. 261: 320–326.
20. Y. Wu, L. Wang, B. Guo, P.X. Ma. "Interwoven Aligned Conductive Nanofiber Yarn/Hydrogel Composite Scaffolds for Engineered 3D Cardiac Anisotropy". ACS Nano. 2017. 11(6): 5646–5659.
21. C. Liu, P.-C. Hsu, H.-W. Lee, M. Ye, et al. "Transparent Air Filter for High-Efficiency PM2.5 Capture". Nat. Commun. 2015. 6(1): 6205.
22. C. Wang, T. Zheng, R. Luo, C. Liu, et al. "In Situ Growth of ZIF-8 on PAN Fibrous Filters for Highly Efficient U(VI) Removal". ACS Appl. Mater. Interfaces. 2018. 10(28): 24164–24171.
23. C. Cleeton, A. Keirouz, X. Chen, N. Radacsi. "Electrospun Nanofibers for Drug Delivery and Biosensing". ACS Biomater. Sci. Eng. 2019. 5(9): 4183–4205.
24. C. Boaretti, L. Pasquini, R. Sood, S. Giancola, et al. "Mechanically Stable Nanofibrous sPEEK/Aquivion® Composite Membranes for Fuel Cell Applications". J. Membr. Sci. 2018. 545: 66–74.
25. S.W. Lee, H.J. Lee, J.H. Choi, W.G. Koh, et al. "Periodic Array of Polyelectrolyte-Gated Organic Transistors from Electrospun Poly(3-hexylthiophene) Nanofibers". Nano Lett. 2010. 10(1): 347–351.
26. D. Papkov, N. Delpouve, L. Delbreilh, S. Araujo, et al. "Quantifying Polymer Chain Orientation in Strong and Tough Nanofibers with Low Crystallinity: Toward Next Generation Nanostructured Superfibers". ACS Nano. 2019. 13(5): 4893–4927.
27. M. Richard-Lacroix, C. Pellerin. "Orientation and Structure of Single Electrospun Nanofibers of Poly(ethylene terephthalate) by Confocal Raman Spectroscopy". Macromolecules. 2012. 45(4): 1946–1953.
28. M. Richard-Lacroix, C. Pellerin. "Orientation and Partial Disentanglement in Individual Electrospun Fibers: Diameter Dependence and Correlation with Mechanical Properties". Macromolecules. 2015. 48(13): 4511–4519.
29. D. Papkov, C. Pellerin, Y.A. Dzenis. "Polarized Raman Analysis of Polymer Chain Orientation in Ultrafine Individual Nanofibers with Variable Low Crystallinity". Macromolecules. 2018. 51(21): 8746–8751.
30. A.W. Laramée, C. Lanthier, C. Pellerin. "Electrospinning of Highly Crystalline Polymers for Strongly Oriented Fibers". ACS Appl. Polym. Mater. 2020. 2(11): 5025–5032.
31. L.M. Bellan, H.G. Craighead. "Molecular Orientation in Individual Electrospun Nanofibers Measured via Polarized Raman Spectroscopy". Polymer. 2008. 49(13): 3125–3129.
32. I. Greenfeld, X. Sui, H.D. Wagner. "Stiffness, Strength, and Toughness of Electrospun Nanofibers: Effect of Flow-Induced Molecular Orientation". Macromolecules. 2016. 49(17): 6518–6530.
33. K. Peng, A. Nain, R. Mirzaeifar. "Tracking the Origins of Size Dependency in the Mechanical Properties of Polymeric Nanofibers at the Atomistic Scale". Polymer. 2019. 175: 118–128.
34. A. Arinstein. "Confinement Mechanism of Electrospun Polymer Nanofiber Reinforcement". J. Polym. Sci., Part B: Polym. Phys. 2013. 51(9): 756–763.
35. A. Dazzi, C.B. Prater, Q. Hu, D.B. Chase, et al. "AFM–IR: Combining Atomic Force Microscopy and Infrared Spectroscopy for Nanoscale Chemical Characterization". Appl. Spectrosc. 2012. 66(12): 1365–1384.
36. Z. Wang, B. Sun, X. Lu, C. Wang, Z. Su. "Molecular Orientation in Individual Electrospun Nanofibers Studied by Polarized AFM–IR". Macromolecules. 2019. 52(24): 9639–9645.
37. R. Dersch, T. Liu, A.K. Schaper, A. Greiner, J.H. Wendorff. "Electrospun Nanofibers: Internal Structure and Intrinsic Orientation". J. Polym. Sci., Part A: Polym. Chem. 2003. 41(4): 545–553.
38. T. Yoshioka, R. Dersch, A. Greiner, M. Tsuji, A.K. Schaper. "Highly Oriented Crystalline PE Nanofibrils Produced by Electric-Field-Induced Stretching of Electrospun Wet Fibers". Macromol. Mater. Eng. 2010. 295(12): 1082–1089.
39. Y.-W. Cheng, H.-A. Lu, Y.-C. Wang, A. Thierry, et al. "Syndiotactic Polystyrene Nanofibers Obtained from High-Temperature Solution Electrospinning Process". Macromolecules. 2010. 43(5): 2371–2376.
40. S. Mollá, V. Compañ. "Polyvinyl alcohol Nanofiber Reinforced Nafion Membranes for Fuel Cell Applications". J. Membr. Sci. 2011. 372(1): 191–200.
41. C. Jia, B. Luo, H. Wang, Y. Bian, et al. "Precise and Arbitrary Deposition of Biomolecules onto Biomimetic Fibrous Matrices for Spatially Controlled Cell Distribution and Functions". Adv. Mater. 2017. 29(35): 1701154.
42. S. Wu, Y. Wang, P.N. Streubel, B. Duan. "Living Nanofiber Yarn-based Woven Biotextiles for Tendon Tissue Engineering Using Cell Tri-Culture and Mechanical Stimulation". Acta Biomater. 2017. 62: 102–115.
43. S.D. Mohan, G.R. Mitchell, F.J. Davis. "Chain Extension in Electrospun Polystyrene Fibres: A SANS Study". Soft Matter. 2011. 7(9): 4397–4404.
44. N. Kimura, H.-K. Kim, B.-S. Kim, K.-H. Lee, I.-S. Kim. "Molecular Orientation and Crystalline Structure of Aligned Electrospun Nylon-6 Nanofibers: Effect of Gap Size". Macromol. Mater. Eng. 2010. 295(12): 1090–1096.
45. E. Zussman, M. Burman, A.L. Yarin, R. Khalfin, Y. Cohen. "Tensile Deformation of Electrospun Nylon-6,6 Nanofibers". J. Polym. Sci., Part B: Polym. Phys. 2006. 44(10): 1482–1489.
46. S.F. Fennessey, R.J. Farris. "Fabrication of Aligned and Molecularly Oriented Electrospun Polyacrylonitrile Nanofibers and the Mechanical Behavior of their Twisted Yarns". Polymer. 2004. 45(12): 4217–4225.
47. M.D. Edwards, G.R. Mitchell, S.D. Mohan, R.H. Olley. "Development of Orientation During Electrospinning of Fibres of Poly(ε-caprolactone)". Eur. Polym. J. 2010. 46(6): 1175–1183.
48. X. Ma, J. Liu, C. Ni, D.C. Martin, et al. "Molecular Orientation in Electrospun Poly(vinylidene fluoride) Fibers". ACS Macro Lett. 2012. 1(3): 428–431.
49. X. Ma, J. Liu, C. Ni, D.C. Martin, et al. "The Effect of Collector Gap Width on the Extent of Molecular Orientation in Polymer Nanofibers". J. Polym. Sci., Part B: Polym. Phys. 2016. 54(6): 617–623.
50. M.V. Kakade, S. Givens, K. Gardner, K.H. Lee, et al. "Electric Field Induced Orientation of Polymer Chains in Macroscopically Aligned Electrospun Polymer Nanofibers". J. Am. Chem. Soc. 2007. 129(10): 2777–2782.
51. T. Kongkhlang, K. Tashiro, M. Kotaki, S. Chirachanchai. "Electrospinning as a New Technique to Control the Crystal Morphology and Molecular Orientation of Polyoxymethylene Nanofibers". J. Am. Chem. Soc. 2008. 130(46): 15460–15466.
52. L. Gong, D.B. Chase, I. Noda, J. Liu, et al. "Discovery of β-Form Crystal Structure in Electrospun Poly[(R)-3-hydroxybutyrate-co-(R)-3-hydroxyhexanoate] (PHBHx) Nanofibers: From Fiber Mats to Single Fibers". Macromolecules. 2015. 48(17): 6197–6205.
53. M. Richard-Lacroix, C. Pellerin. "Raman Spectroscopy of Individual Poly(ethylene oxide) Electrospun Fibers: Effect of the Collector on Molecular Orientation". Vib. Spectrosc. 2017. 91: 92–98.
54. M. Richard-Lacroix, C. Pellerin. "Novel Method for Quantifying Molecular Orientation by Polarized Raman Spectroscopy: A Comparative Simulations Study". Appl. Spectrosc. 2013. 67(4): 409–419.
55. M. Richard-Lacroix, C. Pellerin. "Accurate New Method for Molecular Orientation Quantification Using Polarized Raman Spectroscopy". Macromolecules. 2013. 46(14): 5561–5569.

56. J. Purvis, D.I. Bower. "Molecular Orientation in Poly(ethylene terephthalate) by Means of Laser–Raman Spectroscopy". J. Polym. Sci.: Polym, Phys, Ed. 1976. 14(8): 1461–1484.
57. D.A. Jarvis, I.J. Hutchinson, D.I. Bower, I.M. Ward. "Characterization of Biaxial Orientation in Poly(ethylene terephthalate) by Means of Refractive Index Measurements and Raman and Infra-Red Spectroscopies". Polymer. 1980. 21(1): 41–54.
58. N. Everall. "Optimising Image Quality in 2D and 3D Confocal Raman Mapping". J. Raman Spectrosc. 2014. 45(1): 133–138.
59. J.C. Rodríguez-Cabello, L. Quintanilla, J.M. Pastor. "Fourier Transform Raman Study of the Conformers in Poly(ethylene terephthalate)". J. Raman Spectrosc. 1994. 25(5): 335–344.
60. A.J. Melveger. "Laser-Raman Study of Crystallinity Changes in Poly(ethylene terephthalate)". J. Polym. Sci. A-2: Polym. Phys. 1972. 10(2): 317–322.
61. S. Yang, S. Michielsen. "Orientation Distribution Functions Obtained via Polarized Raman Spectroscopy of Poly(ethylene terephthalate) Fibers". Macromolecules. 2003. 36(17): 6484–6492.
62. N. Everall, P. Tayler, J.M. Chalmers, D. MacKerron, et al. "Study of Density and Orientation in Poly(ethylene terephthalate) Using Fourier Transform Raman Spectroscopy and Multivariate Data Analysis". Polymer. 1994. 35(15): 3184–3192.
63. K.C. Cole, A. Ajji, É. Pellerin. "New Insights into the Development of Ordered Structure in Poly(ethylene terephthalate). 1. Results from External Reflection Infrared Spectroscopy". Macromolecules. 2002. 35(3): 770–784.
64. J. Štokr, B. Schneider, D. Doskočilová, J. Lövy, P. Sedláček. "Conformational Structure of Poly(ethylene terephthalate). Infra-Red, Raman, and NMR Spectra". Polymer. 1982. 23(5): 714–721.
65. C. Pellerin, R.E. Prud'homme, M. Pézolet, B.A. Weinstock, P.R. Griffiths. "Deformation and Relaxation of Polymers Studied by Ultrarapid Scanning FT-IR Spectrometry". Macromolecules. 2003. 36(13): 4838–4843.
66. C. Pellerin, M. Pézolet, P.R. Griffiths. "Time-Resolved Infrared Spectroscopic Studies of Poly(ethylene terephthalate) Deformation". Macromolecules. 2006. 39(19): 6546–6551.
67. N.J. Everall. "Measurement of Orientation and Crystallinity in Uniaxially Drawn Poly(ethylene terephthalate) Using Polarized Confocal Raman Microscopy". Appl. Spectrosc. 1998. 52(12): 1498–1504.
68. C.C.C. Lesko, J.F. Rabolt, R.M. Ikeda, B. Chase, A. Kennedy. "Experimental Determination of the Fiber Orientation Parameters and the Raman Tensor of the 1614 cm^{-1} Band of Poly(ethylene terephthalate)". J. Mol. Struct. 2000. 521(1): 127–136.
69. M.-È. Rousseau, T. Lefèvre, L. Beaulieu, T. Asakura, M. Pézolet. "Study of Protein Conformation and Orientation in Silkworm and Spider Silk Fibers Using Raman Microspectroscopy". Biomacromolecules. 2004. 5(6): 2247–2257.
70. F. Adar, H. Noether. "Raman Microprobe Spectra of Spin-Oriented and Drawn Filaments of Poly(ethylene terephthalate)". Polymer. 1985. 26(13): 1935–1943.
71. A. Garton, D.J. Carlsson, L.L. Holmes, D.M. Wiles. "Trans–Gauche Rotational Isomers in Partially Oriented Poly(ethylene terephthalate) Fibers". J. Appl. Polym. Sci. 1980. 25(7): 1505–1507.
72. X. Li, J. Lin, Y. Zeng. "Electric Field Distribution and Initial Jet Motion induced by Spinneret Configuration for Molecular Orientation in Electrospun Fibers". Eur. Polym. J. 2018. 98: 330–336.
73. V. Chaurey, P.-C. Chiang, C. Polanco, Y.-H. Su, et al. "Interplay of Electrical Forces for Alignment of Sub-100 nm Electrospun Nanofibers on Insulator Gap Collectors". Langmuir. 2010. 26(24): 19022–19026.
74. I. Greenfeld, E. Zussman. "Polymer Entanglement Loss in Extensional Flow: Evidence from Electrospun Short Nanofibers". J. Polym. Sci., Part B: Polym. Phys. 2013. 51(18): 1377–1391.
75. P.K. Bhattacharjee, D.A. Nguyen, G.H. McKinley, T. Sridhar. "Extensional Stress Growth and Stress Relaxation in Entangled Polymer Solutions". J. Rheol. 2002. 47(1): 269–290.